

Chapter 1
Introduction

1.1 Energy Crisis

Energy crisis is a paramount concern in present time, especially in light of the projected global population increase to 9.6 billion by 2050 [1-2]. The energy extracted from oil and gas supplies forms the foundation for industrial, economic and lifestyle growth of the developed world. In industrial agriculture, natural gas and oil supplies are required for inexpensive production of fertilisers, pesticides, industrial machinery planting, cultivating, harvesting, processing, packaging, transportation and marketing. The production of energy and various products from cheap oil have adversely affected our ecosystem [3]. High standard of living leads to higher consumption of fossil fuels. Thus, it can be easily predicted that industrial civilization based on fossil fuels will collapse sooner or later [4]. Global crude oil and natural gas reserves are projected to last up to 41.8 to 60.3 years respectively, based on current production rates [5]. There is a drastic increase in the use of energy in developed areas that is derived from fossil fuels. It has led to an increase in the CO₂ emission in the atmosphere, increasing the global temperature whose negative effects are evident [6]. The rise in global temperature, leads to a rise in sea-level that will immerse the coastal areas. Additionally, sulfur present in fossil fuels, when released into the atmosphere due to fossil fuel usage, results in sulfurous fogs and acid rains. Due to such complications, there is an intensive worldwide discussion aimed at limiting the use of fossil fuels, consequently, reducing CO₂ emissions. Renewable sources are widely recognized as a means of generating clean energy to overcome the aforementioned crisis [7-8]. Recently, World Energy Council (WEC) reported a study declaring that the world energy demand will be 50-80% higher than that of past decade. According to USA Department of Energy (DoE) report, annual energy demand will increase from a current capacity of 363 million kilowatts to 750 million kilowatts within a few years [9]. The world's energy consumption today is estimated to 22 billion kWhyr¹, 53 billion kWh by 2020 [9].

Sustainable development represents the process where the needs of the present are met without compromising the needs of our future generation. The search for alternative energy sources, such as renewable energy, has intensified as conventional energy resources are confirmed to be on the decline [10], and fossil fuels are limited, lasting only another 70-150 years [11]. Renewable energy, derived from natural processes that are continuously replenished, such as sunlight, wind, water, geothermal heat and biomass is being sought [12]. Unlike fossil fuels, renewable energy sources produce minimal greenhouse gas emissions and have a significantly lower environmental footprint. Transitioning to renewable energy is considered a crucial step towards sustainable development and addressing climate change. By investing in and adopting renewable energy techniques, our dependence on fossil fuels can be reduced, environmental damage minimized, and a cleaner and more sustainable energy future promoted.

1.1.1 Various Methods of Renewable Energy Production

Renewable energy sources are derived from the natural and persistent flow of energy that occurs in our immediate environment. They are comprised of bioenergy, direct solar energy, geothermal energy, hydropower, wind and ocean energy [13]. The *Figure 1.1* represents the electrical energy generated from green energy.

- a) **Hydropower:** Harnessed from water moving from higher to lower elevation levels, hydropower is an essential energy source primarily used for turning turbines and generating electricity. Hydropower projects encompass dam projects with reservoirs, run-of-river, and in-stream projects, covering a range of project scales [14].
- b) **Bioenergy:** Derived from biological sources, bioenergy is a renewable energy source. It is an important source of energy that can be used for transport, electricity generation, cooking, and heating. A wide range of different sources attracts electricity from

bioenergy, including forest-by-products such as wood residues; agricultural residues and animal husbandry residue [15].

- c) **Direct solar energy:** The term “direct” solar energy refers to renewable energy technologies that directly harness the sun’s energy. While, some renewable technologies, like wind and ocean thermal, use solar energy after it has been absorbed and transformed on earth into other forms, direct solar energy technologies tap into the sun’s rays directly. Solar energy technology utilizes solar irradiance to generate electricity through photovoltaic systems [16] and concentrating solar power to produce thermal energy, fulfill lighting needs, and potentially create fuels for transportation and other purposes.
- d) **Geothermal energy:** It is obtained naturally from interior of earth’s surface as heat energy source [17].
- e) **Wind energy:** Wind energy have been used since ages for different purpose such as sails, windmills and windpumps. However, it is also used for generating electricity. Major drawback is its dependency on the locations.
- f) **Ocean energy (tide and wave):** The ocean has been part of the development of human civilization lot of minerals have been obtained from the ocean. The tidal-wave energy has been used to generate electricity by turbine in the ocean deep. Moreover, tidal energy used to generate electricity under the ocean as wind turbine and turbine called as tidal turbine. However, the wave energy uses hydraulic pump that’s works with the rise and falls of the waves and thus generates the electricity.
- g) **Electrocatalysis:** We discover the redox reaction and used battery for the generation of the electricity. However, there are lot of drawbacks which holds the usage of electrical batteries which shifts our interest towards hydrogen fuel or water splitting reaction for the generation of electricity. More interest over the water splitting as the bi-product of the reaction is only hydrogen and oxygen gases via hydrogen evolution reaction (HER)

and oxygen evolution reaction (OER). There is a need of a catalyst to promote this reaction which can be electrocatalyst or photocatalyst. The detailed discussion is provided in following sections.

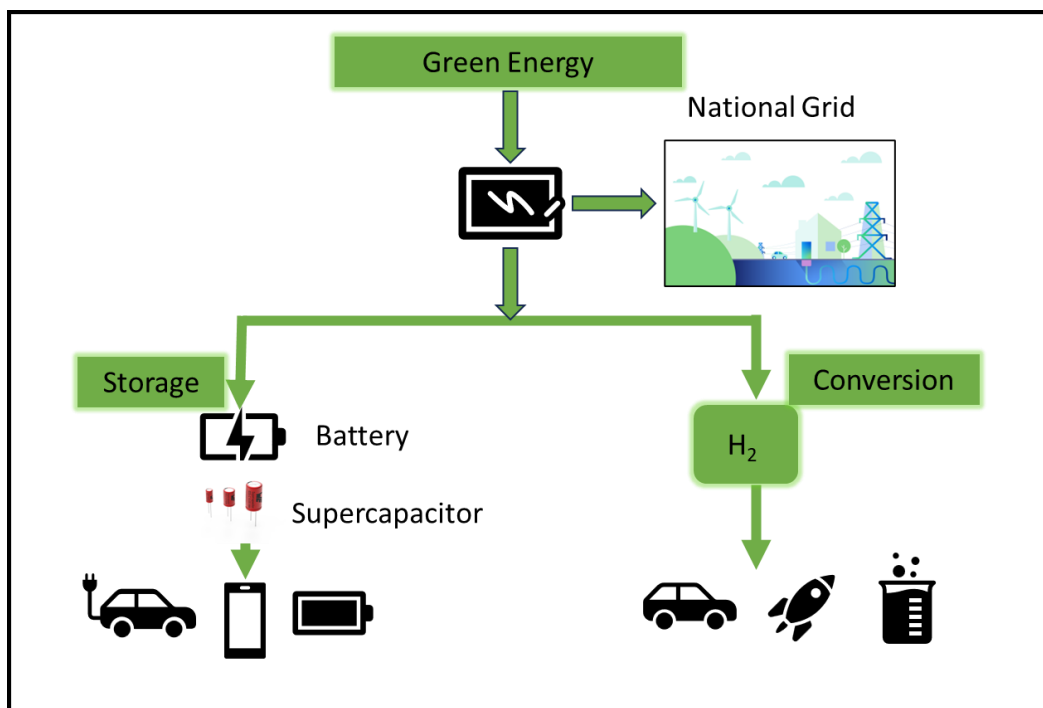


Figure 1.1: Representative scheme for electrical energy harvesting from green energy and excessive electricity storage, conversion, and utilization. Reproduced from [13]

1.2 Electrocatalysis

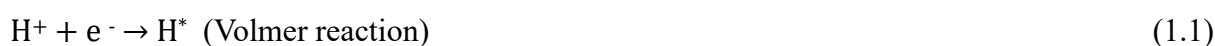
Electrocatalysis is a process that utilizes catalysts to speed up electrochemical reactions. Catalysts play a crucial role in these reactions. For instance, in fuel cells, they facilitate the conversion of fuels like hydrogen or methanol and oxygen into energy resources [18]. Similarly, in electrolyzer, electrocatalysts drive the electrochemical reaction to split water into hydrogen and oxygen using electrical energy. Efficient and affordable electrocatalysts are essential for the advancement of clean energy technologies and the promotion of sustainable energy solutions. Researchers focus on developing innovative materials and structures for

electrocatalysts to enhance their performance and make them more practical for various electrochemical applications. There are several methods to produce hydrogen which is a clean energy source, but among all the methods available electrochemical splitting of water has gained a lot of applause as it has carbon-free byproducts [19,20]. The process of water splitting involves decomposing water into hydrogen gas [21] and oxygen gas through HER and OER, respectively. This decomposition is achieved using an electrical bias or solar power. For this method to be efficient, a highly reactive catalyst is required to promote and accelerate the HER and OER [22]. The catalysts surface-to-volume ratio should be high to ensure an effective splitting process, and it should also be stable, cost-effective, abundant, and capable of enhancing HER and OER activities with lower overpotential [23]. An electrocatalyst ideally should be metallic or a low band gap semiconductor. In addition, photocatalysts that are required to have a band gap in visible light absorption range [24]. Noble metals are considered to be the best candidate to aid the electrochemical water splitting but their scarcity and high-cost limit its usage making way for the discovery of various earth-abundant catalysts. However, challenges remain in terms of searching catalysts that are abundant, inexpensive and stable under the harsh operating conditions of water splitting systems.

1.2.1 Hydrogen Evolution Reaction (HER)

An electrocatalytic HER is a cathodic half-reaction that involves an electrochemical mechanism where reduction of water molecule occurs at the boundary between the electrode and the electrolyte. The production of H₂ depends on the acidity level of the electrolyte: it can be generated through the reduction of either protons (H⁺) or water molecules (H₂O). Both of these pathways encompass a sequence of fundamental chemical processes. There are two consecutive stages (two-electron process) involved in HER activity [25]. Initially, a hydrogen ion (H⁺) adheres to the catalyst's surface, creating an adsorbed hydrogen atom (H*) where the asterisk (*) indicates an active site on the catalyst's surface. This primary step is referred to as

the Volmer step or discharge step (equation 1.1). Following this, an H combines with a hydrogen ion (H^+) and an electron (e^-) to generate H_2 , as shown in (equation 1.2). This stage is known as the Volmer-Heyrovsky step or electrochemical desorption step. Alternatively, H_2 could also be produced via the Tafel step, also termed the chemical desorption step. In this case, two adsorbed hydrogen atoms (H^*) come together on the catalyst's surface and release as H_2 molecule (equation 1.3). The overall HER reaction is illustrated in (equation 1.4), and the standard electrode potential (E°) serves as the baseline for assessing the standard electrode potential in electrochemical reactions [26].



The Sabatier principle [27] underscores the significant role of catalyst- intermediate stage (H^*) interactions in determining the kinetics of the HER [28]. S. Trasatti introduced the first "volcano curve" depicting the relationship between the HER reaction rate on various catalyst surfaces against the energy required for hydride formation by plotting graph [29]. This energy was employed to describe how hydrogen adsorption occurs, given the absence of available experimental or theoretical data on hydrogen adsorption energy (ΔG^H) during that period. In 2004, Nørskov's research team gathered experimental information on exchange current densities for HER across different metals. They calculated corresponding adsorption energies using density functional theory (DFT), subsequently presenting the initial modern volcano plots [30].

1.2.2 Oxygen Evolution Reaction (OER)

OER is the anodic half-reaction in the electrochemical splitting of water. A four-electron reaction mechanism is considered for the explanation of OER where the overall water oxidation reaction is depicted as [31],



At pressure (p) = 1 bar and temperature (T) = 298.15 K, Gibbs free energy difference $\Delta G^0 = 4.92 \text{ eV}$ for this reaction. The above reaction proceeds via the following steps,



In the context of this explanation, the symbol $*$ denotes the catalytic site that is active. Additionally, $* \text{OH}$, $* \text{O}$, and $* \text{OOH}$ represent the different intermediate species attached to the active site. As outlined in the preceding section, under standard conditions, the Gibbs free energy associated with the combination of H^+ and an electron is equal to the Gibbs free energy of producing half a molecule of H_2 . These Gibbs free energies play a crucial role in determining the strength of the bond between the catalyst and the intermediate products involved in the OER process. These interactions are influenced by the electronic characteristics of the active site.

1.3 Emergence of Two-Dimensional Materials: Graphene and Transition Metal Chalcogenides

Graphene stands as the inaugural example of an authentic two-dimensional (2D) atomic crystal [32]. It possesses distinct electronic, optical, and mechanical attributes, and has

garnered extensive attention in various fields such as spanning electrocatalysis [33], photocatalysis [34], and conventional heterogeneous catalysis [35]. Notably, deviations from graphene's flawless hexagonal arrangement—such as dislocations, vacancies, edges, impurities, and functional groups easily alter its structural and electronic characteristics and enhance its catalytic characteristics [36]. Graphene, an atomic crystal in 2D form, is composed of a single layer of carbon atoms exhibiting sp^2 hybridization [37]. This fundamental structural unit serves as a building block for diverse carbon allotropes such as one-dimensional (1D) carbon nanotubes, and zero-dimensional (0D) fullerenes [37]. In recent times, there has been a surge of interest in other 2D atomic crystals and their potential catalytic applications due to its diverse properties [38]. Numerous layered materials, including MoS_2 and WS_2 , have long been utilized as catalysts in their three-dimensional (3D) configurations. However, the marked shifts in the electronic makeup of 2D materials compared to their bulk 3D structures, coupled with the feasibility of making chemical and structural adjustments, introduce novel prospects for leveraging these 2D materials in diverse chemical reactions.

2D transition metal dichalcogenides (TMDs) like MoS_2 and WS_2 nanosheets have garnered significant research attention. The marked alterations in the electronic configuration of these 2D materials compared to their 3D counterparts (for example, a monolayer of MoS_2 functions as a direct-bandgap semiconductor, whereas multiple layers would result in an indirect bandgap [39]) and the potential to modify their chemical and mechanical characteristics open up fresh avenues for utilizing them as catalysts in numerous chemical reactions. The catalytic prowess of these 2D TMDs stems from the sulfur (S) sites located at their edges [40]. Beyond MoS_2 and WS_2 , 2D nanosheets composed of other layered TMDs, such as SnS_2 and SnS , have gained escalating interest, particularly within the realm of photocatalysis [41]. When compared to their bulk counterparts, X-ray absorption fine structure spectroscopy and DFT calculations often unveil structural deviations in these semiconducting nanosheets. For SnS_2 and SnS nanosheets,

such structural variations result in a conspicuous augmentation of the density of states in the valence band at the edges, relative to their bulk counterparts [41]. This amplified density of states contributes to heightened optical absorption and the mobility of charge carriers generated by light, consequently augmenting the efficacy of charge transfer processes. There is a constant growth in the study of these TMDs leading to new parameters and applications.

1.4 Catalytic Properties of 2D Transition Metal Chalcogenides

The realm of materials science has been captivated by the class of transition metal chalcogenides (TMCs), as it holds immense potential in various applications such as sensors, energy conversion, and energy storage [42]. Moreover, the landscape of electrochemical energy conversion, particularly involving transition metal-based electrocatalysts, has garnered noteworthy attention over the past few years. This is attributed to their remarkable blend of high activity, cost-effectiveness, and ease of customization. Among these electrochemical processes, the division of water through electrocatalysis, encompassing HER and OER [42,43] has emerged as a pivotal arena for research. However, the practical implementation of water splitting technology hinges on the identification of stable and effective catalysts that can facilitate both HER and OER by reducing energy barriers and enhancing Faraday efficiency. Conventional catalysts often feature Pt as a standout HER performer, while Ir and RuO₂ exhibit prowess in OER. Nevertheless, the prohibitive cost and limited stability associated with these precious-metal catalysts impede their widespread commercial adoption. Enter TMCs, a relatively recent entrant to the scene, demonstrating unparalleled efficiency in HER and OER across a broad pH spectrum. In general, TMCs can have various stoichiometries such as MX, MX₂ and of MX₃. Here, MX represents transition metal chalcogenides, MX₂ represents transition metal dichalcogenides whereas MX₃ denotes transition metal trichalcogenides etc. where M indicates transition metal and X chalcogen respectively. In terms of crystal phases,

the TMDs can exhibit different phases, with the two main heterogeneous polymorphic structures being the octahedral coordination phase (1T), which shows metallic properties, and the trigonal prismatic phase (2H), which gives semiconducting properties. A third distorted octahedral (1T') phase can also be observed and this phase has semi-metallic characteristics [44].

1.4.1 Experimental Studies

Following the groundbreaking discovery of graphene, a multitude of novel 2D materials have surfaced [45], including TMDs such as MoS₂ and WS₂ nanosheets. These TMDs have emerged as captivating and efficient electrocatalytic materials, characterized by substantial surface areas and robust chemical stability [45]. They not only facilitate water electrolysis but also boast intriguing semiconductor properties, which can be manipulated and harnessed in photoelectrochemical cells. The ability to engineer TMDs with a spectrum of conductivities—ranging from semiconductors [46] to metallic-like conduction and superconductors [47]—confers adaptability for diverse applications.

Notably, the electrochemical activity of these 2D TMDs such as MoS₂, WS₂, MoSe₂ and WSe₂ predominantly stems from the edge sites [48], given that their basal planes are electrochemically inert. Introducing strain or defects on these basal planes enhances catalytic activity by creating more active sites, including kinks, terraces, corner atoms, chalcogenide and transition metal vacancies, point defects, and grain boundaries, facilitating rapid electron transfer [48]. MoS₂, for instance, has been extensively studied as an electrocatalyst for the HER, standing out as the most widely investigated among the TMDs [49-50]. Various synthesis techniques have been employed, such as dispersion of MoS₂ sheets in solvents [51] followed by deposition, chemical vapor deposition [52], or physical vapor deposition [53] onto substrates. Efforts have also been made to enhance HER activity through non-metallic doping, like N [54] and O [55], as well as co-doping strategies [56]. Zhang et al. [57] provided evidence

of how N doping can effectively enhance the conductivity of the basal plane in MoS₂. Similarly, Wang et al. [56] revealed that the typically unresponsive basal plane can be rendered active through the synergistic co-doping of N and F. Utilizing DFT calculations, Deng et al. [58] arrived at the conclusion that metal atoms found in groups IV to VIII of the periodic table—namely, V, Ti, Fe, Mn, Cr—tend to form bonds with six S atoms. In contrast, metal atoms belonging to groups IX to XII, including Pt, Ag, Pd, Co, and Ni, display a preference for bonding with only four S atoms. This disparity in bonding patterns can lead to variations in the HER activity, given that unsaturated S atoms promote the adsorption of hydrogen atoms. The researchers predicted that metal atoms from groups 4 to 8 would exhibit lower activity in the HER process, whereas doping with elements from groups IX to XII could enhance HER performance. In line with their DFT calculations, the authors determined that doped MoS₂'s HER activity followed the order Pt > Co > Ni, aligning well with experimental measurements [58].

Transition metal diselenides (TMSe₂), a subclass of 2D materials, have recently exhibited higher electrochemical activity for H₂ generation compared to their disulfide counterparts. Se atom's higher metallic property, coupled with its enhanced electroactive edge sites, makes it more advantageous than S [59]. Moreover, its wider interlayer spacing enables efficient ion insertion and extraction in electrolytes. In acidic environments [60], MoSe₂ demonstrates superior electrocatalytic activity for HER compared to MoS₂. Gholamvand et al. [61] conducted a comparative analysis of HER activity in acidic conditions, evaluating solution-processed films of MoS₂, WS₂, MoSe₂, WSe₂, MoTe₂, and WTe₂ nanosheets. They concluded that the performance hierarchy followed the order of selenide > sulfide > telluride, with MoSe₂ demonstrating the most exceptional performance. Similarly, Tang et al. [62], in their comparison of MoS₂ and MoSe₂, determined that MoSe₂ outperforms MoS₂ as an electrocatalyst for HER. This observation was attributed to the Gibbs energy change associated

with the hydrogen adsorption process on the electrocatalyst. Typically, a value approaching 0 eV signifies a favourable HER electrocatalyst. Intriguingly, DFT calculations affirmed that MoSe₂ displays a favourable adsorption energy in acidic environments. However, in alkaline solutions, MoSe₂ encounters challenges due to unfavourable water adsorption and dissociation steps. To achieve efficient HER activity under these conditions, supplementary components are frequently introduced to enhance performance. However, in alkaline solutions, additional components like CoSe are often combined with MoSe₂ to optimize HER efficiency. In the realm of photoelectrochemical water splitting, certain 2D post-TMDs, like vertically aligned SnS₂ nanosheets [63], have shown promise as photoanodes. Nonetheless, often hybrid systems involving TMDs and other semiconducting materials, particularly Si, are employed to enhance hydrogen production. Hybrid configurations, such as Si/TMD photocathodes, exhibit impressive photoelectrochemical performance, demonstrating the multifaceted potential of these materials.

1.4.2 Theoretical Studies

DFT stands out as a widely recognized and successful quantum mechanical tool extensively employed to analyze and predict the properties of bulk to nanomaterials [64]. Its reputation is rooted in its predictive prowess, particularly when direct experimental exploration becomes challenging due to factors like cost, intricate technical demands posed by extreme conditions (such as high pressures and temperatures), or the investigation of hazardous substances or nuclear radiation [65]. In contrast to classical methodologies, DFT offers superior capabilities by embracing a quantum mechanical framework to elucidate interactions within quantum systems. These encompass the behaviour of electrons within periodic systems, electron-phonon interactions, quasi-particle dispersions, and non-equilibrium states. This approach delves into the intricate dynamics of electrons within materials by solving the many-body-time-independent Schrödinger equation.

Showkat et al. have extended the utility of the boron sheet through functionalization, introducing diverse elemental dopants like C, N, P, S and Li. Their investigation involved determining adsorption energy when hydrogen and oxygen molecules were positioned top of doped sites on the boron sheet. This is particularly significant as boron is the lightest element capable of forming extensive covalently bonded materials. Predictions based on first-principles electronic structure calculations have theoretically anticipated 2D boron sheet, categorized as α , β , and γ types [66]. Tang and Ismail et al. [67,68] studied that the α -sheet represents the most stable ultrathin nanostructure due to its highest cohesive energy. Notably, density of states (DOS) calculations has indicated the metallic nature of considered systems. Optical spectra revealed absorption peaks at lower photon energies. In terms of H and O adsorption, the calculations unveiled strong binding to both pristine and functionalized boron surfaces. Among various dopant, C emerged as the most promising candidate for demonstrating good HER and OER activities, positioning it favourably as a lightweight catalytic material [69].

TMDs with the stoichiometry MX_2 (M: Mo, V, W, Pt; X: S, Se) have garnered attention as effective non-precious catalysts for clean hydrogen production via water splitting. However, their inactive basal planes compared to their edge sites present a challenge. Recent advancements include the synthesis of Janus MoSSe , a sandwiched structure that predicts increased catalytic activity through strain, external electric fields, and vacancy creation. Som et al. [70] studied the electronic band gap calculations which revealed the potential for ZrS_2 and ZrSSe to serve as photo-catalysts, while ZrSe_2 exhibited a low band gap suitable for electrocatalysis. By evaluating Gibbs free energy, Nb-ZrSe_2 emerged as the most suitable candidate for HER, followed by Pt-ZrS_2 , Nb-ZrSSe , Nb-ZrS_2 , and ZrSSe . The functionalization of these systems improved their basal activity, with Nb dopant ZrSe_2 demonstrating enhanced catalytic performance.

Additionally, theoretical investigations have highlighted the photocatalytic potential of PtS₂ and WS₂ monolayers, complemented by promising catalytic activity when coupled with reduced graphene oxide [71] and WS₂ nano flakes [72]. This study builds on these findings, aiming to enhance the HER activity of PtS₂ and WS₂ through DFT-based electronic structure calculations. The incorporation of foreign elements like Ag, Au, Hg, Pd, Ir, Rh, and Rh has been explored to optimize catalytic activity. In particular, Pd-doped WS₂ exhibited good HER activity among all the systems considered [73].

1.5 Enhancement in the Catalytic Efficiency

The literature survey indicates that the creation of defects and doping are most effective techniques for enhancing the HER/OER activity of various 2D materials. Subsequent section, presents defect and doping discussion.

1.5.1 Doping

To surmount the constraints inherent to traditional 2D semiconductors, a prevalent strategy involves chemically modifying the material through doping. Doping entails the introduction of foreign atomic species into the host 2D material at a specified concentration. This practice hinges on the characteristics of the chemical dopant, encompassing its size, charge, and inherent nature. Dopants can exhibit n-type behaviour, contributing electrons to the host, or p-type behaviour, accepting electrons from the host. Notably, alkali metals are recognized as n-type dopants, while non-metals like boron and chlorine serve as exemplary p-type dopants. Additionally, the process of doping can be categorized as interstitial, substitutional, and chemical [13]. Interstitial doping refers to the incorporation of dopant atoms in the interstitial spaces between the crystal lattice, rather than becoming part of the lattice itself. Conversely, substitutional doping involves integrating dopant atoms into the lattice, perturbing the inherent structure of the 2D material. Experimentally, chemical doping can be accomplished by

adsorbing dopant atoms or molecules onto the surface of the 2D material. The interaction between the adsorbates and the material's surface induces a transfer of surface charge, influenced by the nature of the atoms or molecules. This, in turn, leads to modifications in the electronic structure of the 2D material.

1.5.2 Defect

Likewise, in scenarios where a constituent atom of the host structure is absent or displaced from its initial position, it signifies the generation of a defect within the host framework. These defects exert a pivotal influence on the manipulation of 2D material properties, encompassing both structural and electronic facets [75]. This influence arises from the alterations in the lattice constant and crystal configuration that defects introduce. The variation in lattice constant can be ascribed to the strain imposed on the host material upon defect incorporation, concurrently leading to adjustments in the overall charge dynamics of the system.

1.6 Research Objectives

The aim of this proposed work is to investigate the structural, electronic and optical properties of various metal chalcogenides. Our aim will provide the better understanding of physical and chemical properties of metal chalcogenides and detailed study of doping induced characteristic of metal chalcogenides. The main focus of this work is to investigate the effect of doping on electronic and optical properties to analyze the change in catalytic effect of materials. Our aim is to provide the understanding of enhancement of catalytic effect before and after tuning properties of metal chalcogenides. However, the specific objectives of the present work are following:

1. First the determination of ground state and geometry structure of metal chalcogenides using DFT simulations.

2. To investigate the possible electronic properties of metals chalcogenides and modification electronic properties of metal chalcogenides for surface phenomena via charge transfer induced that is by doping dopant, applying strain or by creating defect.
3. To study the interaction and stabilization of the metal chalcogenides at specific sites with foreign atoms and various intermediates such as hydrogen and oxygen.
4. The calculation of work function to understand surface phenomena that is interaction between adsorbate (metal chalcogenides) and adsorbent (hydrogen or oxygen atoms). As the change in work function is related to presence of minute amount of contamination on a monolayer or occurrence of surface reaction
5. The calculation of optical properties of given metal chalcogenides helps us to know potential applications of these materials such as photocatalyst or electrocatalyst for HER.

1.7 Structure of the Present Thesis

The rest of this thesis is organized as follows:

A theoretical description of computational methodology used throughout the work is presented in **Chapter 2**. In this chapter, theoretical concepts which are the basis of DFT are presented and discussed. In particular, all quantities which help to calculate the electronic, dynamical and catalytic properties of 2D materials on the basis of DFT are discussed. We present all basic ideas of many body problems, Born-Oppenheimer, Hartree and Hartree-Fock approximations followed by density-based method and Kohn-Sham equation in chapter 2. Moreover, the use of plane wave to represent electron wave functions and density needed to deal with valance and core electrons implemented in Quantum Espresso code are discussed.

We also discuss the Grimme's dispersion correction which is important not only to predict correct adsorption energies but also important to consider van der Waals interaction which is important for layered systems.

Chapter 3, discusses stability and electronic properties of 2D honeycomb structure of tin diselenide (SnSe_2) and its catalytic activity for HER and OER using dispersion corrected DFT simulations. From our results, we found that the SnSe_2 has indirect band gap of 0.80 eV and shows potential as photocatalyst for HER activity. Furthermore, we have tuned the structural, electronic and catalytic properties of SnSe_2 by substitutional doping of Na, K and Ca atoms. We found that on doping of Na, K and Ca dopants the semiconducting nature of pristine SnSe_2 becomes metallic in nature. The Gibbs free energy for pristine and Na, K and Ca doped systems for hydrogen atom adsorption is 0.79 eV, -0.29 eV, -1.29 eV and 0.72 eV respectively. Also, the Gibbs free energy for pristine and Na, K and Ca doped systems for oxygen atom adsorption is -0.69 eV, -0.54 eV, -1.72 eV and -0.45 eV respectively. Our results show that the Na-doped SnSe_2 monolayer is more suited for HER catalyst as the Gibbs free energy is close to zero. The Ca-doped SnSe_2 monolayer is the better candidate for OER catalyst, followed by Na-doped and pristine SnSe_2 monolayers.

Chapter 4, includes the study carried out by employing defect engineering on SnSe_2 . We have analyzed the effect of different defects on the catalytic properties of SnSe_2 . We investigated its catalytic activity for HER using DFT simulations. For an accurate prediction of H adsorption on SnSe_2 for HER, we have applied dispersion correction (DFT-D3). From our calculations, we observed that creating defects on various sites indeed improves the catalytic efficiency. We have studied effect of various types of defects on electronic and catalytic behaviours on considered systems. Among various defects, monoselenide vacancy (V_{Se}), diselenide vacancy (V_{Se_2}), vacancy complex of Sn and nearby three diselenide atoms (V_{SnSe_3}) and vacancy complex of Sn and nearby three diselenide pairs (V_{SnSe_6}) are stable configurations

which are considered for further study. The V_{Se} defect shows promising catalytic activity when it occupies the hollow site, with a favourable ΔG^H value of 0.40 eV. In contrast, the Sn and Se sites exhibit slightly less favourable values of 0.54 eV and 0.48 eV, respectively. When we consider the V_{Se_2} defect, the ΔG^H values suggest that the Se site is the most favourable for catalysis compared to both the Sn site and the hollow site. Moving on to the V_{SnSe_3} defect, both Se sites and hollow sites demonstrate favourable ΔG^H values of 0.27 eV and 0.19 eV, respectively, while the Sn site shows a slightly less favourable value of -0.22 eV. Lastly, in the case of the V_{SnSe_6} defect, the hollow site proves to be more efficient for H adsorption compared to the Sn site. Among all the defects, it becomes clear that the hollow site in V_{SnSe_3} is the most promising candidate for HER, followed by the Se sites in V_{SnSe_3} and V_{SnSe_6} , respectively.

Chapter 5, discusses the structural, electronic and catalytic activity for HER of pristine and defected hafnium-based transition metal chalcogenide (HfX; X=S₂, SSe, Se₂) monolayers using dispersion corrected DFT simulations. From our calculations, we found that the band gap of HfS₂, HfSSe, and HfSe₂ is 1.28 eV, 0.98 eV and 0.68 eV respectively. Thereafter, we calculated the Gibbs free energy of H adsorption at different sites of all pristine monolayers, we observed that all three pristine monolayers are not suitable for HER activity. Previously, defect engineering of MoS₂ is shown to be an effective tool for enhancing the basal activity of the MoS₂ monolayer. Therefore, we have studied two mono defects of Hf and S/Se for better catalytic activity through band gap modulation. We found that Hf defect leads to the lower Gibbs free energy compared to the S/Se defect in HfS₂, HfSSe and HfSe₂ monolayer. The lowest Gibbs free energy is at the Hollow site (0.22 eV) for the Hf-defect HfSe₂ monolayer, S-edge site (0.25 eV) for the Hf-defected Janus monolayer and Hf site (0.03 eV) for Hf defected HfS₂ monolayer. We observed that basal plane activity enhances for Hf defected HfS₂ monolayer. In addition, this chapter includes discussions of band structure, partial density of states (PDOS) and charge transfer in order to understand the HER activity.

Chapter 6 serves as a conclusive overview, encapsulating the pivotal findings and prospective applications obtained from this thesis. It also delves into the prospects for future research in the domain of water splitting, focusing on the utilization of 2D materials.

References

1. UN News, “United Nations Department of economic and social affairs,” [Online]. 13 june (2013)[Accessed 18 january 2014].
2. Pathak, S., *Int. J. Eng. Res. Appl*, 2014, **4**, pp.845-851,.
3. “Earth-A Graphic look at the state of the world,” The Global Education Project, [Online]. Available: <http://www.theglobaleducationproject.org/earth/energy-supply.php>.
4. J.O. Bockris, A.K.N. Reddy, A. K. N, *Springer Private Limited, New York*, 2014.
5. F. Behrouzi, M. Nakisa, A. Maimun and Y. M. Ahmed, *Renewable and Sustainable Energy Reviews*, 2016, **62**, 1270–1281.
6. Z. Qin, Y. Chen, Z. Huang, J. Su, Z. Diao and L. Guo, *The Journal of Physical Chemistry C*, 2016, **120**, 14581–14589.
7. J. D. Benck, T. R. Hellstern, J. Kibsgaard, P. Chakthranont and T. F. Jaramillo, *ACS Catal*, 2014, **4**, 3957–3971.
8. M.-R. Gao, Y.-F. Xu, J. Jiang and S.-H. Yu, *Chem Soc Rev*, 2013, **42**, 2986.
9. H. H. Lean and R. Smyth, *Appl Energy*, 2014, **132**, 168–177.
10. K. Y. Foo, *Renewable and Sustainable Energy Reviews*, 2015, **51**, 1477–1498.
11. K. Sopian and W. R. Wan Daud, *Renew Energy*, 2006, **31**, 719–727.
12. S.-S. TONG, X.-J. WANG, Q.-C. LI and X.-J. HAN, *Chinese Journal of Analytical Chemistry*, 2016, **44**, 1447–1457.
13. Q. Zhu, Y. Qu, D. Liu, K. W. Ng and H. Pan, *ACS Appl Nano Mater*, 2020, **3**, 6270–6296.
14. Asumadu-Sarkodie, S., Owusu, P.A. and Jayaweera, M., (2015).
15. Urban, F. and Mitchell, T., (2011).
16. P. A. Owusu and S. Asumadu-Sarkodie, *Cogent Eng*, 2016, **3**, 1167990.
17. E. Barbier, *Renewable and Sustainable Energy Reviews*, 2002, **6**, 3–65.
18. M. MOMIRLAN and T. VEZIROGLU, *Int J Hydrogen Energy*, 2005, **30**, 795–802.
19. J. E. Trancik, *Nature*, 2014, **507**, 300–302.
20. F. Pincella, K. Isozaki and K. Miki, *Light Sci Appl*, 2014, **3**, e133–e133.
21. T. Shinagawa, A. T. Garcia-Esparza and K. Takanabe, *Sci Rep*, 2015, **5**, 13801.

22. J. Lee, S. Kang, K. Yim, K. Y. Kim, H. W. Jang, Y. Kang and S. Han, *J Phys Chem Lett*, 2018, **9**, 2049–2055.
23. S. H. Mir, S. Chakraborty, P. C. Jha, J. Wärnå, H. Soni, P. K. Jha and R. Ahuja, *Appl Phys Lett*, 2016, **109**(5).
24. S. H. Mir, S. Chakraborty, J. Wärnå, S. Narayan, P. C. Jha, P. K. Jha and R. Ahuja, *Catal Sci Technol*, 2017, **7**, 687–692.
25. B. E. Conway and B. V. Tilak, *Electrochim Acta*, 2002, **47**, 3571–3594.
26. H. P. Lehmann, X. Fuentes-Arderiu and L. F. Bertello, *Pure and Applied Chemistry*, 1996, **68**, 957–1000.
27. P. Quaino, F. Juarez, E. Santos and W. Schmickler, *Beilstein Journal of Nanotechnology*, 2014, **5**, 846–854.
28. R. Parsons, *Transactions of the Faraday Society*, 1958, **54**, 1053.
29. S. Trasatti, *J Electroanal Chem Interfacial Electrochem*, 1972, **39**, 163–184.
30. J. K. Nørskov, T. Bligaard, A. Logadottir, J. R. Kitchin, J. G. Chen, S. Pandalov and U. Stimming, *J Electrochem Soc*, 2005, **152**, J23.
31. J. K. Nørskov, J. Rossmeisl, A. Logadottir, L. Lindqvist, J. R. Kitchin, T. Bligaard and H. Jónsson, *J Phys Chem B*, 2004, **108**, 17886–17892.
32. K. S. Novoselov, A. K. Geim, S. V. Morozov, D. Jiang, Y. Zhang, S. V. Dubonos, I. V. Grigorieva and A. A. Firsov, *Science (1979)*, 2004, **306**, 666–669.
33. E. Antolini, *Appl Catal B*, 2012, **123–124**, 52–68.
34. X. An and J. C. Yu, *RSC Adv*, 2011, **1**, 1426.
35. B. F. Machado and P. Serp, *Catal. Sci. Technol.*, 2012, **2**, 54–75.
36. D. Deng, L. Yu, X. Pan, S. Wang, X. Chen, P. Hu, L. Sun and X. Bao, *Chemical Communications*, 2011, **47**, 10016.
37. A. K. Geim and K. S. Novoselov, *Nat Mater*, 2007, **6**, 183–191.
38. K. S. Novoselov, D. Jiang, F. Schedin, T. J. Booth, V. V. Khotkevich, S. V. Morozov and A. K. Geim, *Proceedings of the National Academy of Sciences*, 2005, **102**, 10451–10453.
39. K. F. Mak, C. Lee, J. Hone, J. Shan and T. F. Heinz, *Phys Rev Lett*, 2010, **105**, 136805.
40. T. F. Jaramillo, K. P. Jørgensen, J. Bonde, J. H. Nielsen, S. Horch and I. Chorkendorff, *Science (1979)*, 2007, **317**, 100–102.
41. Y. Sun, H. Cheng, S. Gao, Z. Sun, Q. Liu, Q. Liu, F. Lei, T. Yao, J. He, S. Wei and Y. Xie, *Angewandte Chemie International Edition*, 2012, **51**, 8727–8731.
42. M. Nath, U. De Silva, H. Singh, M. Perkins, W. P. R. Liyanage, S. Umaphathi, S. Chakravarty and J. Masud, *ACS Appl Energy Mater*, 2021, **4**, 8158–8174.

43. X. Cao, J. E. Medvedeva and M. Nath, *ACS Appl Energy Mater*, 2020, **3**, 3092–3103.
44. M. S. Sokolikova, P. C. Sherrell, P. Palczynski, V. L. Bemmer and C. Mattevi, *Nat Commun*, 2019, **10**, 712.
45. T. Yu and C. B. Breslin, *J Electrochem Soc*, 2020, **167**, 037514.
46. S. Manzeli, D. Ovchinnikov, D. Pasquier, O. V. Yazyev and A. Kis, *Nat Rev Mater*, 2017, **2**, 17033.
47. A. Hamill, B. Heischmidt, E. Sohn, D. Shaffer, K.-T. Tsai, X. Zhang, X. Xi, A. Suslov, H. Berger, L. Forró, F. J. Burnell, J. Shan, K. F. Mak, R. M. Fernandes, K. Wang and V. S. Pribiag, *Nat Phys*, 2021, **17**, 949–954.
48. S. Ramki, R. Sukanya, S.-M. Chen, M. Sakthivel and J. Y. Wang, *New Journal of Chemistry*, 2019, **43**, 17200–17210.
49. A. K. Kunhiraman, M. Bradha and R. A. Rakkesh, *J Mater Res*, 2021, **36**, 4141–4153.
50. D. Voiry, M. Salehi, R. Silva, T. Fujita, M. Chen, T. Asefa, V. B. Shenoy, G. Eda and M. Chhowalla, *Nano Lett*, 2013, **13**, 6222–6227.
51. Y. Li, K. Yin, L. Wang, X. Lu, Y. Zhang, Y. Liu, D. Yan, Y. Song and S. Luo, *Appl Catal B*, 2018, **239**, 537–544.
52. M. A. Lukowski, A. S. Daniel, F. Meng, A. Forticaux, L. Li and S. Jin, *J Am Chem Soc*, 2013, **135**, 10274–10277.
53. D. Kong, H. Wang, J. J. Cha, M. Pasta, K. J. Koski, J. Yao and Y. Cui, *Nano Lett*, 2013, **13**, 1341–1347.
54. R. Li, L. Yang, T. Xiong, Y. Wu, L. Cao, D. Yuan and W. Zhou, *J Power Sources*, 2017, **356**, 133–139.
55. Y. Deng, Z. Liu, A. Wang, D. Sun, Y. Chen, L. Yang, J. Pang, H. Li, H. Li, H. Liu and W. Zhou, *Nano Energy*, 2019, **62**, 338–347.
56. Y. Wang, S. Liu, X. Hao, J. Zhou, D. Song, D. Wang, L. Hou and F. Gao, *ACS Appl Mater Interfaces*, 2017, **9**, 27715–27719.
57. P. Zhang, B. Xu, G. Chen, C. Gao and M. Gao, *Electrochim Acta*, 2018, **270**, 256–263.
58. J. Deng, H. Li, J. Xiao, Y. Tu, D. Deng, H. Yang, H. Tian, J. Li, P. Ren and X. Bao, *Energy Environ Sci*, 2015, **8**, 1594–1601.
59. S. Ramaraj, M. Sakthivel, S.-M. Chen and K.-C. Ho, *Anal Chem*, 2019, **91**, 8358–8365.
60. A. Ambrosi, Z. Sofer and M. Pumera, *Chemical Communications*, 2015, **51**, 8450–8453.
61. Z. Gholamvand, D. McAteer, C. Backes, N. McEvoy, A. Harvey, N. C. Berner, D. Hanlon, C. Bradley, I. Godwin, A. Rovetta, M. E. G. Lyons, G. S. Duesberg and J. N. Coleman, *Nanoscale*, 2016, **8**, 5737–5749.

-
62. H. Tang, K. Dou, C.-C. Kaun, Q. Kuang and S. Yang, *J. Mater. Chem. A*, 2014, **2**, 360–364.
 63. A. Y. S. Eng, A. Ambrosi, Z. Sofer, P. Šimek and M. Pumera, *ACS Nano*, 2014, **8**, 12185–12198.
 64. P. J. Hasnip, K. Refson, M. I. J. Probert, J. R. Yates, S. J. Clark and C. J. Pickard, *Philosophical Transactions of the Royal Society A: Mathematical, Physical and Engineering Sciences*, 2014, **372**, 20130270.
 65. A. Jain, Y. Shin and K. A. Persson, *Nat Rev Mater*, 2016, **1**, 15004.
 66. X. Wu, J. Dai, Y. Zhao, Z. Zhuo, J. Yang and X. C. Zeng, *ACS Nano*, 2012, **6**, 7443–7453.
 67. H. Tang and S. Ismail-Beigi, *Phys Rev B*, 2010, **82**, 115412.
 68. H. Tang and S. Ismail-Beigi, *Phys Rev Lett*, 2007, **99**, 115501.
 69. S. H. Mir, S. Chakraborty, P. C. Jha, J. Wärnå, H. Soni, P. K. Jha and R. Ahuja, *Appl Phys Lett*, , DOI:10.1063/1.4960102.
 70. N. N. Som and P. K. Jha, *Int J Hydrogen Energy*, 2020, **45**, 23920–23927.
 71. H. L. Zhuang and R. G. Hennig, *The Journal of Physical Chemistry C*, 2013, **117**, 20440–20445.
 72. L. Cheng, W. Huang, Q. Gong, C. Liu, Z. Liu, Y. Li and H. Dai, *Angewandte Chemie International Edition*, 2014, **53**, 7860–7863.
 73. S. H. Mir, S. Chakraborty, J. Wärnå, S. Narayan, P. C. Jha, P. K. Jha and R. Ahuja, *Catal Sci Technol*, 2017, **7**, 687–692.
 74. Z. Lin, B. R. Carvalho, E. Kahn, R. Lv, R. Rao, H. Terrones, M. A. Pimenta and M. Terrones, *2d Mater*, 2016, **3**, 022002.